

# Corrosion Behavior of Austenitic Stainless Steels in Oxidizing and Reducing Gases Relevant to Oxyfuel Power Plants

P. HUCZKOWSKI,<sup>1,4</sup> S. NAJIMA,<sup>1,2</sup> A. CHYRKIN,<sup>3</sup>  
and W.J. QUADAKKERS<sup>1</sup>

1.—Forschungszentrum Jülich GmbH, Institute of Energy and Climate Research (IEK-2), 52425 Jülich, Germany. 2.—Central Research Institute of Electric Power Industry, Nagasaki, Yokosuka 240-0196, Japan. 3.—Materials Microstructure, Department of Physics, Chalmers University of Technology, 412 96 Göteborg, Sweden. 4.—e-mail: p.huczkowski@fz-juelich.de

The oxidation behavior of three austenitic stainless steels was studied at 650°C up to 1000 h. The selected materials (S304HCu, TP347HFG, and Sanicro 25) were exposed to an atmosphere simulating oxyfuel combustion, and the results compared with the behavior in a test gas with addition of CO, thus simulating locally occurring reducing operating conditions. For the 18% Cr steels (S304HCu and TP347HFG), lower corrosion rates were generally found in reducing than oxidizing gas. As might be expected based on its substantially higher Cr content, Sanicro 25 showed lower oxidation rates than the two 18% Cr steels in the oxyfuel gas. However, the opposite was the case in the reducing gas. The higher Ni content resulted in formation of a mixed sulfide/oxide outer layer, which adversely affected the formation of a protective chromia scale, resulting in a higher corrosion rate than for the 18% Cr steels.

## INTRODUCTION

Oxyfuel technology is a promising option for significantly reducing CO<sub>2</sub> emissions in future modern coal-fired power plants.<sup>1</sup> The oxyfuel process is based on pulverized coal combustion using pure oxygen instead of air.<sup>2</sup> As oxyfuel flue gas contains mostly CO<sub>2</sub> and H<sub>2</sub>O, CO<sub>2</sub> separation is much easier than in conventional power plants.<sup>3</sup>

In an oxyfuel plant, the heat-exchanging metallic components are exposed to a flue gas that contains much higher CO<sub>2</sub> and H<sub>2</sub>O contents than conventional flue gases.<sup>4</sup> In the temperature range of 600–650°C, austenitic stainless steels are considered as candidate alloys for boiler tubes due to their good corrosion resistance against the service environments and high creep strength.<sup>5,6</sup>

Austenitic steels with Cr concentrations of around 18% are reported to form multilayered, Fe-rich oxide scales when exposed to H<sub>2</sub>O (CO<sub>2</sub>)-rich gases above 600°C,<sup>7</sup> whereby the actual behavior is strongly affected by alloy grain size and surface

treatment.<sup>8</sup> For 25% Cr austenitic steels and NiCr-base alloys, much lower oxidation rates were observed. However, high water vapor content in combination with intentionally added oxygen in the test atmosphere may affect protective scale formation due to enhanced formation of volatile chromium species.<sup>5,7,9</sup>

For given sulfur content in coal, the SO<sub>2</sub> concentration in oxyfuel flue gas may be higher than in conventional combustion environments,<sup>4</sup> although this depends on the oxyfuel concept applied. In the case of 18% Cr austenitic steels, it was shown that presence of SO<sub>2</sub> in the gas resulted in minor internal Cr sulfide formation beneath the external scale. Presence of SO<sub>2</sub> also decreased the extent of C uptake, which was explained by preferential adsorption of sulfur at inner surfaces.<sup>10</sup>

Another technological challenge in an oxyfuel plant is the combustion process, because both the fuel and oxidant are supposed to be consumed simultaneously in this process. In some cases, incomplete combustion accompanied by CO formation may occur locally, resulting in reducing operating conditions in the plant.<sup>11</sup> In previous studies, it was shown that, in reducing conditions (gas

A. Chyrkin was formerly at Forschungszentrum Jülich GmbH, Institute of Energy and Climate Research (IEK-2), 52425 Jülich, Germany.

composition Ar-25% $H_2O$ -60% $CO_2$ -1% $CO$ -0.5% $SO_2$ ), austenitic 18% Cr steels form chromia scales with local formation of Fe-rich nodules during exposure at 650°C and 700°C. Traces of sulfur were found in the inner scale, at the scale–alloy interface, and in the form of Cr sulfide precipitates in the subscale region, especially at alloy grain boundaries.<sup>12,13</sup>

This study presents the corrosion behavior of three austenitic stainless steels currently being considered as construction materials for heat-exchanging components in oxyfuel plants. The main aim of this study is to elucidate differences in material performance under oxidizing and reducing gases simulating oxyfuel conditions. This study did not address the effect of deposits.

## EXPERIMENTAL PROCEDURES

Three different austenitic stainless steels were used as test materials: S304HCu, TP304HFG, and Sanicro 25. The detailed chemical composition of the materials is presented in Table I. For oxidation experiments, samples of 20 mm × 10 mm with thickness of 2 mm were prepared from delivered plates or tubes. Specimens were exposed to Ar- $H_2O$ - $CO_2$ - $O_2$ - $SO_2$  gas (henceforth designated oxyfuel gas) and compared with the behavior in Ar- $H_2O$ - $CO_2$ - $CO$ - $SO_2$  (designated as reducing oxyfuel gas hereinafter). The name “reducing gas” is frequently used in practice and is applied here to simplify the description of the mentioned atmosphere throughout the paper. However, it should be mentioned that, based on thermodynamic considerations presented in previous studies,<sup>13</sup> the mentioned gas will actually not be reducing for all elements present in the studied alloys. The exact composition of the test gases is listed in Table II. The composition of the oxyfuel gas was based on calculations presented in Ref. 4, assuming use of dried lignite as fuel and an oxyfuel process including flue gas recirculation. The oxidizing and reducing test gases were virtually identical apart from the fact that the oxygen added in the former was replaced by CO to obtain the latter. The test temperature of 650°C was selected based on the typically envisaged service temperature of austenitic steels in real applications.<sup>1–5,14</sup> Prior to oxidation tests, the specimens were ground to P1200 surface finish using silicon carbide paper

and degreased in ethanol. Oxidation experiments were performed for 1000 h in alumina reaction tubes, with mass changes measured discontinuously every 250 h, i.e., after specimen cooling to room temperature.

The oxide scales formed during oxidation were analyzed using light optical microscopy and scanning electron microscopy with energy- and wavelength-dispersive x-ray spectroscopy (SEM with EDX/WDX) (Zeiss Supra 50 VP and Merlin). For cross-section analyses, specimens were mounted in epoxy resin after coating with a thin gold layer then electroplating with nickel. The nickel layer mechanically supported the oxide scale during further metallographic preparation and additionally improved the contrast between the oxide scale and mounting material during SEM characterization.

## RESULTS

According to the mass change data for the three studied austenitic steels during discontinuous exposure to the oxyfuel gas at 650°C (Fig. 1a), the highest oxidation rate was found for TP347HFG steel followed by S304HCu and Sanicro 25. In the reducing oxyfuel gas (Fig. 1b), the opposite behavior was found; i.e., higher corrosion rates were observed for Sanicro 25 than for TP347HFG and S304HCu.

Figure 2 shows metallographic cross-sections of the studied austenitic steels after 1000 h of oxidation at 650°C in the two test atmospheres. These results confirm the relative differences in corrosion resistance as derived from the weight change data. Figure 3 presents the oxide scale morphology and x-ray mappings of the scale formed on TP347HFG exposed to oxyfuel gas. The metallographic cross-sections presented in Figs. 2c and 3 (for TP347HFG), combined with the data from previous studies<sup>10,13</sup> (for S304HCu), reveal that, in oxyfuel gas, both steels form a similar double-layer oxide scale consisting of Fe-rich oxide (hematite) in the outer part and Cr-rich oxide in the inner part of the scale. EDX analysis (Fig. 3 and data in Refs. 10 and 13) also showed that internal Cr-rich sulfides form in the subscale zone within the alloy. This is clearly accompanied by Cr depletion in the surrounding alloy matrix up to a substantial depth.

**Table I. Composition (in wt.%) of studied alloys analyzed by inductively coupled plasma optical emission spectroscopy (ICP-OES) and infrared analysis**

Steel	wt.%								Others
	Fe	Cr	Ni	Mn	Si	C	N	Nb	
S304HCu	Bal.	18.7	8.7	0.7	0.2	0.09	0.11	0.4	0.02Al, 2.8Cu
TP347HFG	Bal.	18.3	11.3	1.6	0.4	0.09	0.04	0.8	–
Sanicro 25	Bal.	22.6	25.5	0.5	0.2	0.06	0.23	0.5	0.06Al, 2.9Cu, 1.5Co, 3.7 W

**Table II. Chemical composition of the used simulated oxyfuel gases in vol.%**

Gas designation	Composition (vol.%)						
	Ar	N <sub>2</sub>	CO <sub>2</sub>	H <sub>2</sub> O	O <sub>2</sub>	SO <sub>2</sub>	CO
Oxyfuel gas	11.5	–	60	25	3	0.5	–
Reducing oxyfuel gas	13.5	–	60	25	–	0.5	1

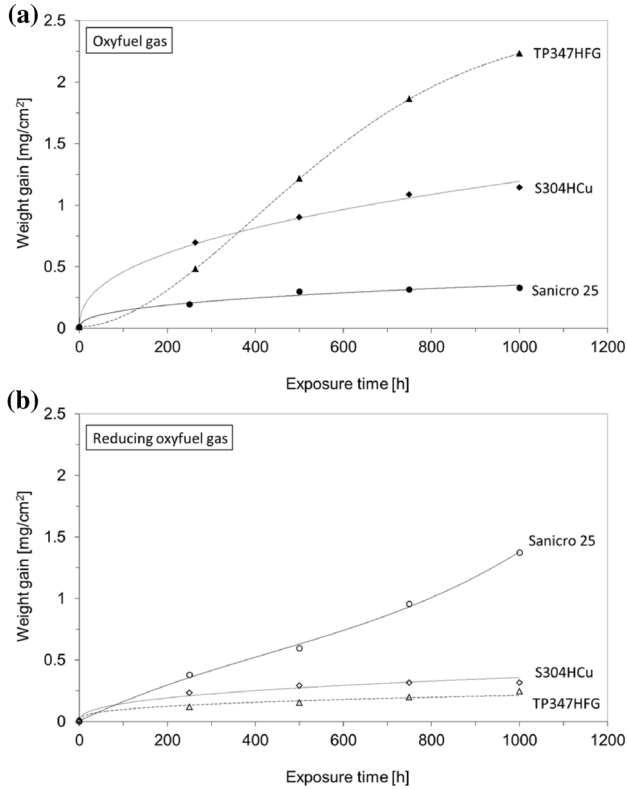


Fig. 1. Weight change of the three investigated steels during 1000 h of discontinuous exposure at 650°C to (a) oxyfuel and (b) reducing oxyfuel gas.

The metallographic cross-section presented in Fig. 2e combined with the EDX mappings presented in Fig. 4 reveal that Sanicro 25 exposed to oxyfuel gas formed a Cr-rich oxide scale (mainly consisting of Cr<sub>2</sub>O<sub>3</sub>) accompanied by local formation of internal Cr sulfides and W-rich precipitates. In the regions of local internal sulfide formation, minor amounts of Fe- and Cu-containing oxides formed on top of the chromia.

After exposure to reducing oxyfuel gas, the scale on S304HCu and TP347HFG was found to consist mainly of Cr<sub>2</sub>O<sub>3</sub>. However, the alloys started to form double-layer scales on some areas of the samples with iron-rich nodules, mainly containing magnetite in the outer layer (Figs. 2b, d and 5, Ref. 13). In these areas, local precipitates of internal Cr-rich sulfides accompanied by internal oxidation (especially for TP347HFG) were found. In the reducing

oxyfuel gas, Sanicro 25 formed a layer of Cr-rich oxide, which was accompanied by formation of an external oxide/sulfide mixture (Cr and Fe oxide/Ni and Cu sulfide) and a wide zone of extensive internal oxidation/sulfidation (Figs. 2f and 6). Tungsten-containing precipitates were also detected in the alloy in the zone of internal oxidation/sulfidation.

## DISCUSSION

### External Scale Formation

When analyzing the mechanisms of external scale formation for the three exposed austenitic steels, it is important to consider which phases (oxides, sulfides, sulfates, etc.) are thermodynamically stable under the experimental conditions used in the present study. Such considerations have already been presented and extensively discussed in previous papers for low-Cr steels, martensitic 9–12% Cr steels, austenitic steels, and Ni-base alloy 617<sup>10,13</sup> and are not discussed here in detail. The austenitic steels S304HCu and TP347HFG formed oxides in contact with both studied gases (Fig. 2), in agreement with the results in Ref. 10. Sulfides and sulfates of iron and chromium are not stable under the experimental conditions used here.<sup>10</sup> This is not the case for sulfides/sulfates of nickel. However, apparently, the nickel content in the steels was too low for nickel sulfate (in oxyfuel gas) or sulfide (in reducing oxyfuel gas) to form at the gas–scale interface. The formation of the much thinner scale on S304HCu and TP347HFG in the reducing than in the oxyfuel gas (Fig. 2) may be related to the smaller thermodynamic driving force, accompanied by a slow growth rate of Fe-rich oxides in the low-*p*<sub>O<sub>2</sub></sub> gas.<sup>13</sup>

The lower corrosion rate of Sanicro 25 in oxyfuel gas can be explained by the much higher Cr content (~22 wt.%) in this steel compared with that in the 18% Cr steels S304HCu and TP347HFG. The higher chromium content of Sanicro 25 leads to formation of a surface layer consisting virtually exclusively of Cr<sub>2</sub>O<sub>3</sub> with only minor amounts of outer Fe- and Cu-containing oxides (Fig. 4). Subscale Cr sulfide formation was also found for the alloy (Fig. 4). However, the remaining Cr content in the steel matrix between the sulfide precipitates was found by EDX to be approximately 10%, i.e., higher than the 7–8% in the case of the 18% Cr steels. Apparently, the higher remaining Cr matrix concentration was sufficient to retain the protective chromia scale

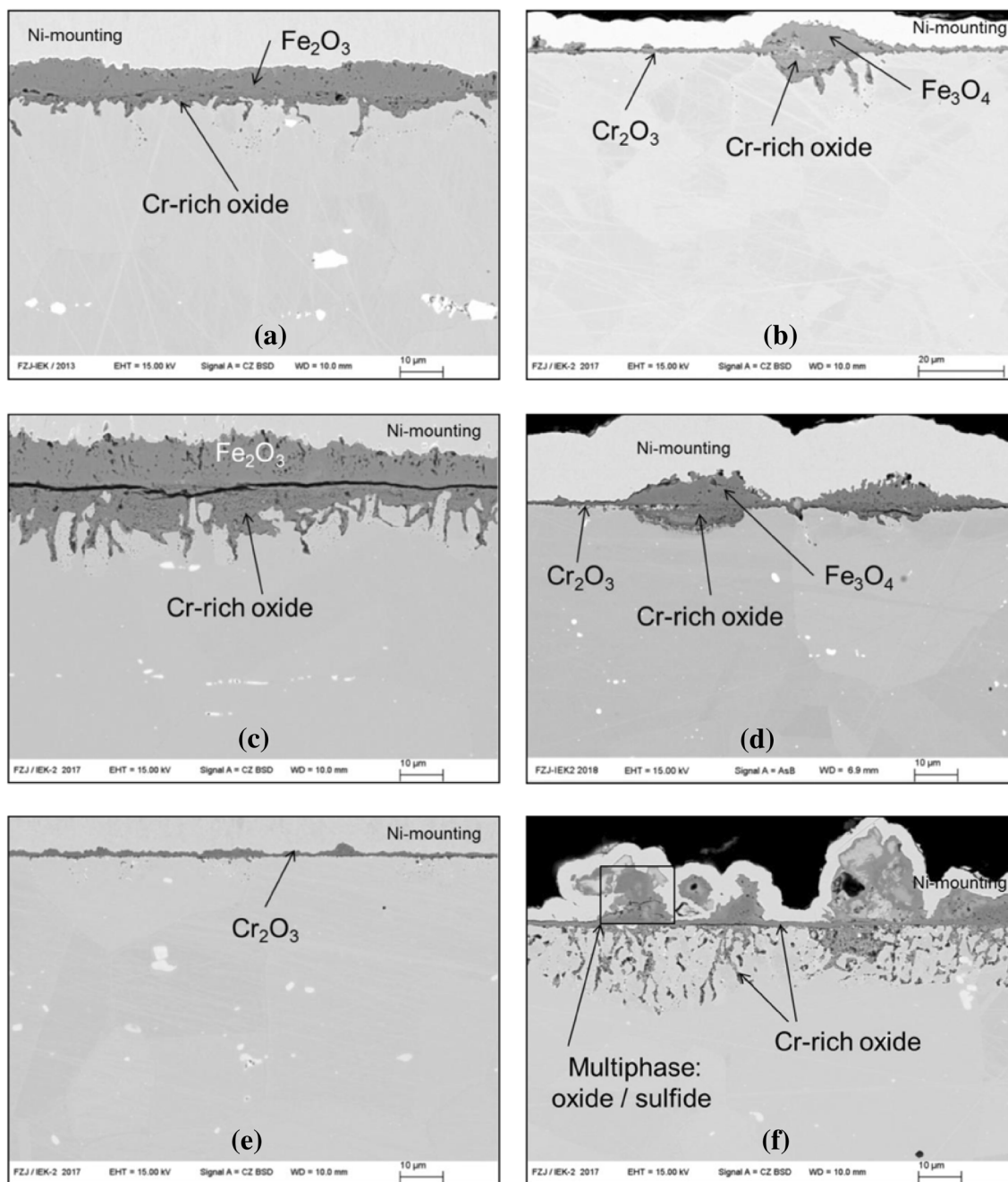


Fig. 2. Metallographic cross-sections (SEM images) of the three investigated steels after 1000 h of exposure at 650°C to oxyfuel and reducing oxyfuel gas: (a) S304H in oxyfuel gas, (b) S304H in reducing oxyfuel gas, (c) TP347HFG in oxyfuel gas, (d) TP347HFG in reducing oxyfuel gas, (e) Sanicro 25 in oxyfuel gas, and (f) Sanicro 25 in reducing oxyfuel gas; boxed area in (f) shows outer mixed sulfide/oxide.

growth, at least up to the maximum exposure time of 1000 h, and only minor amounts of Fe- and Cu-containing oxide were formed locally.

In reducing oxyfuel conditions, Ni- and Cu-containing sulfides were found in contact with the gas together with oxide phases on Sanicro 25. In previous studies,<sup>13</sup> it was found that Ni-base alloy 617 formed a heterogeneous surface scale consisting of oxides and Ni/Co-containing sulfides in contact

with the gas after exposure to reducing oxyfuel gas in the temperature range of 550–700°C; the tendency for formation of this external sulfide appeared to exhibit a maximum at 650°C. Apparently, formation of these rapidly growing sulfide phases suppressed formation of the protective Cr oxide, which would be thermodynamically stable over Cr sulfide.<sup>13</sup> Apparently, in Sanicro 25, the enhanced tendency for external sulfide formation due to the

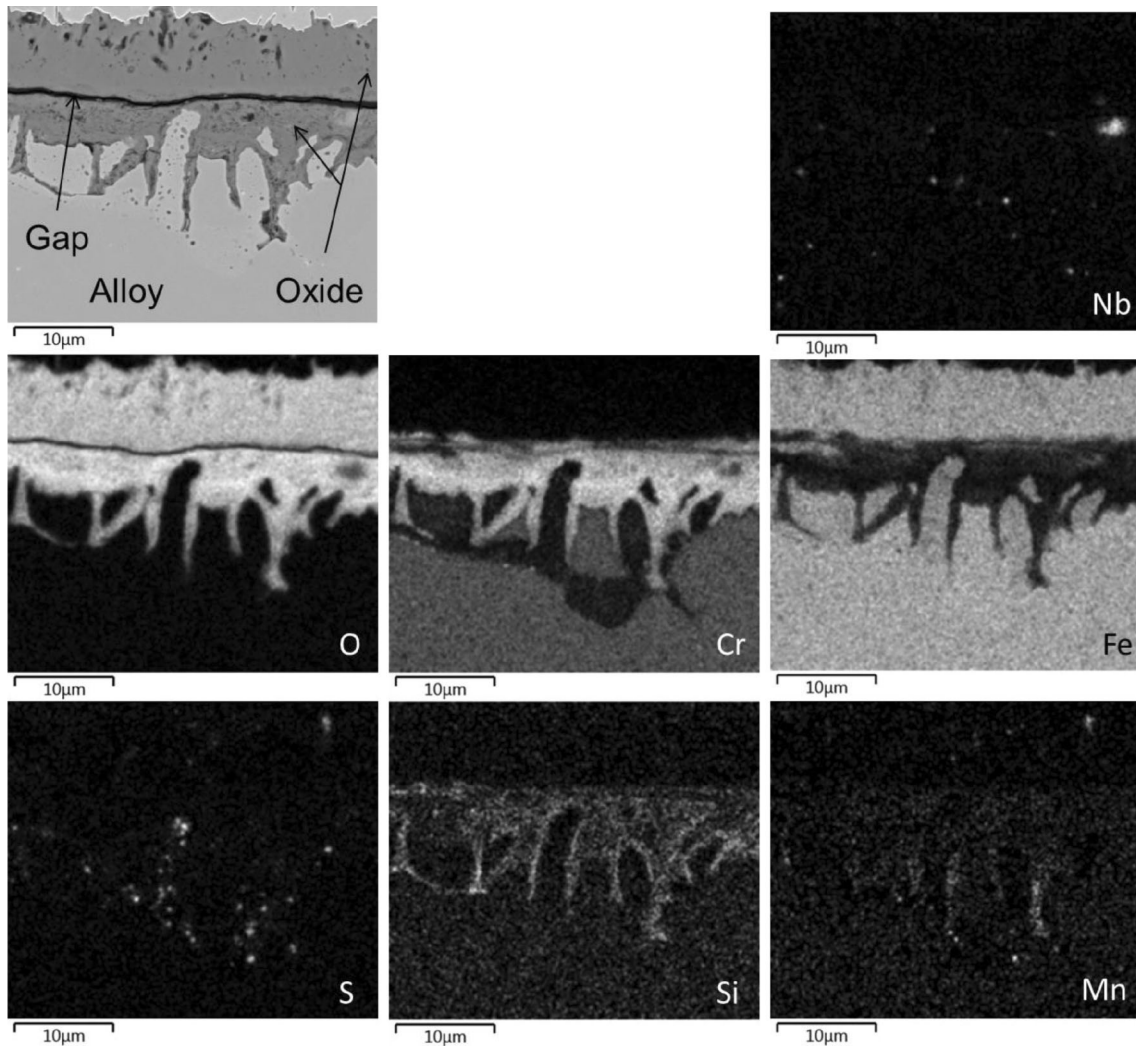


Fig. 3. Metallographic cross-section showing BSE image (upper left) and EDX element maps for austenitic steel TP347HFG after 1000 h of oxidation at 650°C in oxyfuel gas.

higher nickel content compared with TP347HFG and S304HCu could not be suppressed by enhanced protective chromia scale formation as a result of the higher Cr content of approximately 22%.

### Internal Corrosion

The results show that the low concentration (0.5 vol.%) of SO<sub>2</sub> in both gases was sufficient to cause formation of sulfur-rich internal corrosion products for all three alloys, even if external oxide layers formed. Evidently, sulfur penetrates the external scale, forming a sulfide phase as internal precipitates, where the oxygen potential is very low. As extensively explained by several authors (see, e.g., Refs. 15 and 16), molecular transport of SO<sub>2</sub> through scale allows (mainly Cr-rich) sulfides to form beneath the oxide scale, although they are not stable in thermodynamic equilibrium with the gas. The regions of internal sulfide formation clearly exhibited Cr depletion in the surrounding alloy

matrix (Figs. 3–5). EDX point analyses on the 18% Cr steels revealed that the remaining Cr content in the steel matrix in regions of internal sulfide formation was as low as 7–8 wt.%. This subscale Cr depletion in the steel matrix is likely responsible for the formation of Fe- (and Cu-)based oxides in the outer scale, as found for S304HCu and TP347HFG after exposure to oxyfuel gas (entire scale, Fig. 3 for TP347 HFG) and in reducing oxyfuel gas (Fe-rich nodules, Fig. 5 for TP347HFG).

Examining the cross-sections of TP347HFG exposed to oxyfuel gas and of Sanicro 25 exposed to reducing oxyfuel gas, extensive internal oxidation of Cr was found to accompany internal sulfidation (Fig. 2c and f). The same effect but to a much lesser extent was also observed for S304HCu in oxidizing gas (Fig. 2a). Zhou et al.<sup>17</sup> reported that depletion of chromium in the internal corrosion zone by internal sulfidation led to a shift from external to internal oxidation of Cr. Choi and Stringer<sup>18</sup> postulated that breakdown of the Cr<sub>2</sub>O<sub>3</sub> scale due to penetration of

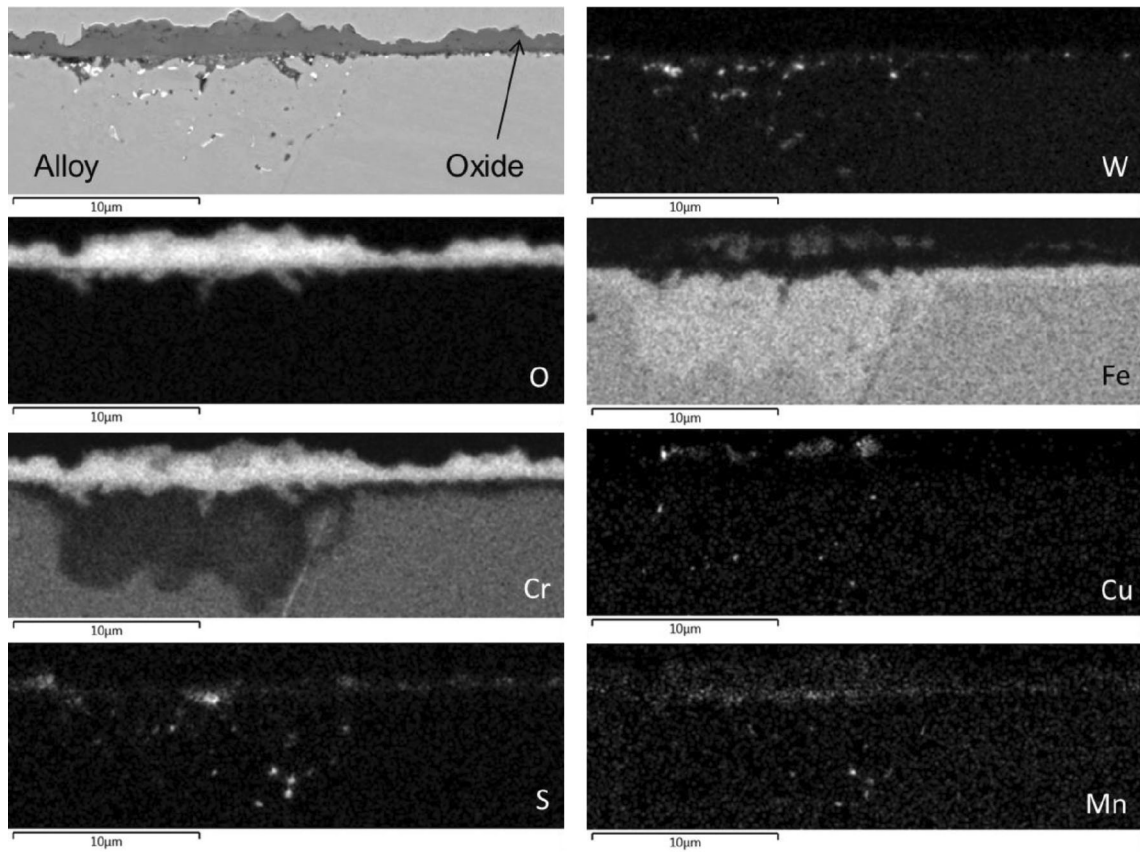


Fig. 4. Metallographic cross-section showing BSE image (upper left) and EDX element maps for austenitic steel Sanicro 25 after 1000 h of oxidation at 650°C in oxyfuel gas.

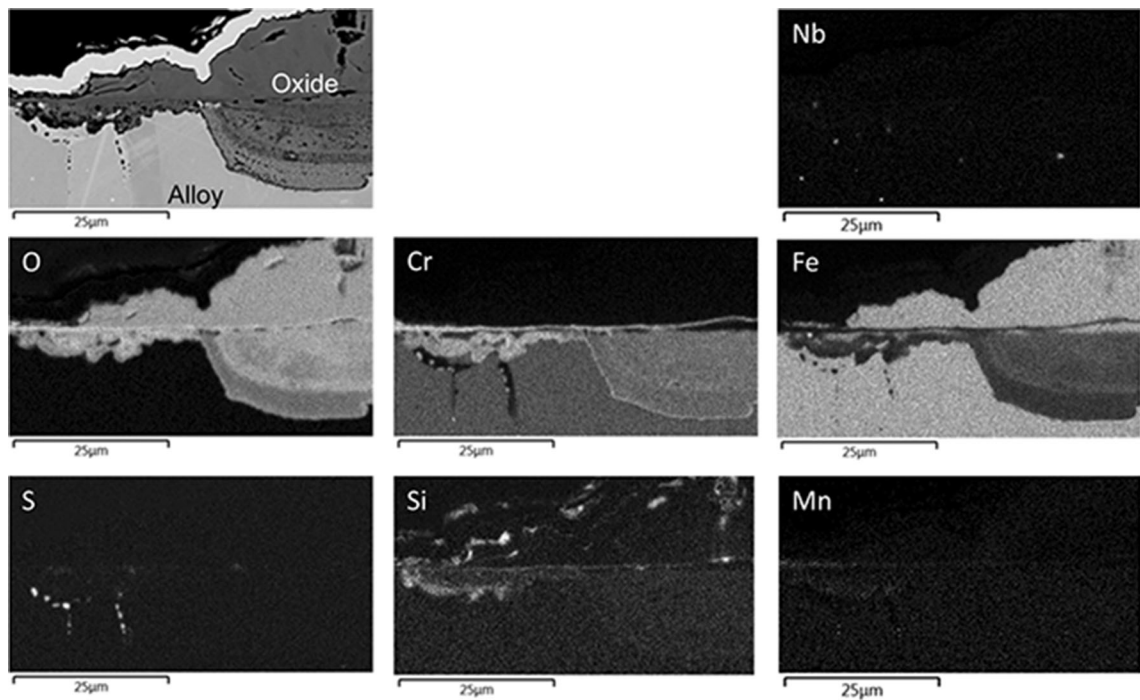


Fig. 5. Metallographic cross-section showing BSE image (upper left) and EDX element maps for austenitic steel TP347HFG after 1000 h of oxidation at 650°C in reducing oxyfuel gas.

sulfur to the alloy–scale interface was initiated by development of a critical microstructure in the subsurface of the alloy. The critical microstructure corresponded to a relatively coarse distribution of internal chromium sulfide precipitates which intersected the alloy–scale interface. It was proposed that not only did the internal sulfides tie up the chromium, but that their subsequent oxidation resulted in a porous, and hence permeable, oxide.<sup>19</sup> A mechanism by which internally formed Cr sulfide is subsequently oxidized, especially along grain boundaries, is a likely explanation for the “finger-like” inner scale morphology clearly observed for S304HCu and especially for TP347HFG after exposure to oxyfuel gas (Fig. 2a and c).

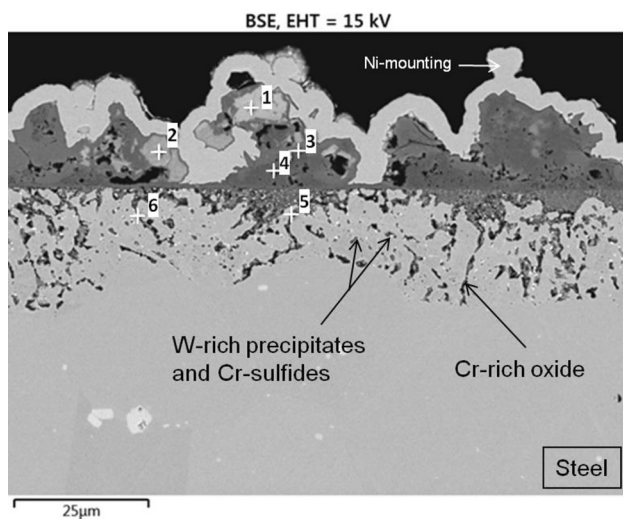


Fig. 6. Metallographic cross-section (SEM/BSE) of austenitic steel Sanicro 25 after 1000 h of reaction in reducing oxyfuel gas at 650°C. Phases as derived from EDX analysis: 1: Cu sulfide, 2: Ni sulfide 3: Fe oxide, 4: Cr oxide, 5: Cr oxide, 6: Cr sulfide.

The most pronounced zone of internal corrosion was found for Sanicro 25 after exposure to reducing gas (Figs. 2f and 6). Here, the internal corrosion zone also consisted mainly of Cr sulfides and oxides. Based on the considerations above, it is believed that the outer mixed oxide/sulfide scale allows more molecular ingress of SO<sub>2</sub> than scales mainly consisting of (Cr-rich) oxides. The resulting enhanced internal Cr sulfide formation accompanied by extensive matrix Cr depletion leads to stepwise oxidation of the Cr sulfides, resulting in the internal corrosion morphology seen in Fig. 6. It is interesting to note that the internal corrosion zone contained very fine, W-rich precipitates. This type of precipitate was also found in subsurface zones after long-term steam oxidation.<sup>20</sup> The precipitate formation is thus not directly caused by ingress of sulfur but is the result of matrix Cr depletion. The shift in phase equilibria resulting in formation of the W-rich  $\mu$ -phase precipitates was discussed in Ref. 20.

### Difference in Behavior of 18% Cr Steels in Oxyfuel Gas

An interesting question to consider is why the thickening rate of the (inner) scale in the oxyfuel gas was substantially lower for S304HCu than for TP347HFG (Fig. 2a and c). As these two alloys do not substantially differ in terms of Cr content (Table I), this effect may be explained by differences in the concentrations of minor alloying elements. The main difference here is the presence of Cu in S304HCu and higher concentrations of Si, Nb, and Mn in TP347HFG. Addition of approximately 3 wt.% copper to S304HCu steel allows formation of stable copper precipitates, contributing to the high creep strength of the steel.<sup>6</sup> Kim et al.<sup>6</sup> showed that Cu additions in austenitic stainless steel induce Cu-containing spinel oxides on the top surface after long-term oxidation in air with 20%

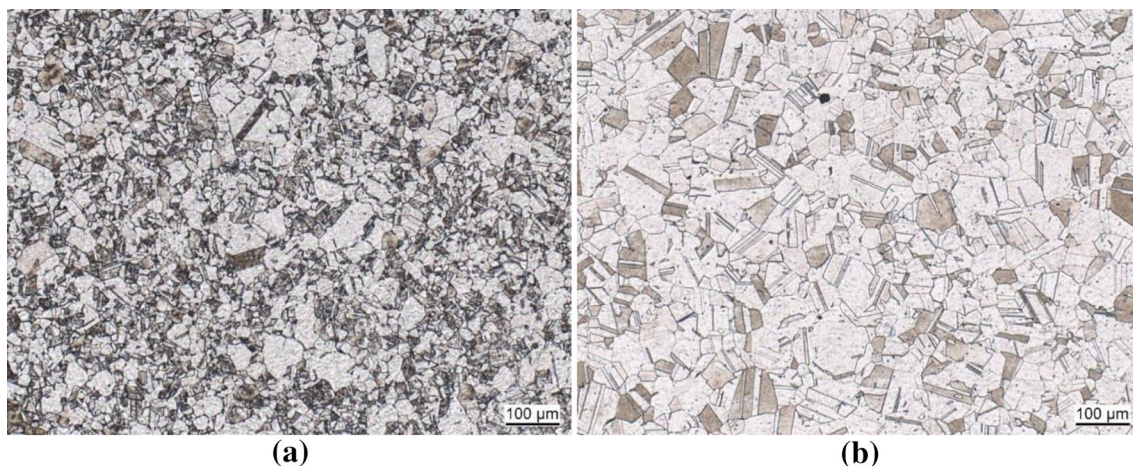


Fig. 7. Etched metallographic cross-sections (light optical microscopy) of (a) S304HCu and (b) TP347HFG in as-received condition (electrolytic etching in H<sub>2</sub>SO<sub>4</sub> solution).

water vapor. The same effect was observed in the present study (see also Refs. 10 and 13) for S304HCu in oxyfuel gas. It cannot be determined with certainty whether this had a substantial effect on the scaling rate.

The back-scattered electron (BSE) image of TP347HFG in Fig. 3 reveals a certain enrichment of Si in the inner part of the scale formed in oxyfuel gas. The question is whether this Si enrichment could adversely influence the overall corrosion rate of the steel compared with S304HCu. It has frequently been described in literature (see, e.g., Ref. 21) that silicon additions may actually improve the oxidation resistance of Fe-Cr and Fe-Cr-Ni alloys. It is claimed that SiO<sub>2</sub> layers that form at the scale-alloy interface act as diffusion barriers, thus significantly reducing the chromia layer growth rates. On the other hand, Huczkowski et al.<sup>22</sup> found that minor additions of Si (and Al) tended to increase the growth rate of the Cr-rich oxide scales on high-Cr ferritic steels for solid oxide fuel cell (SOFC) applications. Presence of Si (and Al) impurities led to internal oxide precipitates of silica and alumina. The volume increase caused by the formation of these internal oxide precipitates resulted in formation of metal protrusions into the oxide scale, thereby causing an increase in the oxidation rate of the steel. Considering the morphology of the Si-containing oxide phases in Fig. 3, it is unlikely that the latter effect could be responsible for the higher oxidation rate of TP347HFG compared with S304HCu.

In the present study, presence of Nb-rich carbides was detected in the matrix of the investigated alloys, in agreement with findings in previous studies.<sup>10,13</sup> Nb-rich carbides, if present near the surface, may be the trigger for duplex scale formation upon the chromia scale. The higher amount of Nb in TP347HFG may thus cause faster onset of duplex scale formation compared with S304HCu. However, based on the observations on the materials studied here, it appears that such mixed scale formation triggered by Nb-rich precipitates was localized and did not spread over the entire specimen surface.

In addition, the Mn content in the TP347HFG alloy is higher than that in S304HCu. Kim et al.<sup>6</sup> observed minor amounts of Mn in the outer oxide layer during exposure of model Cu-containing austenitic steels. A similar effect is observed for Mn-containing ferritic stainless steels, where formation of a (MnCr)<sub>3</sub>O<sub>4</sub> spinel phase is frequently observed on top of protective chromia.<sup>22,23</sup> However, under the present conditions, Mn was observed in the inner part of the scale or near the scale-alloy interface and was mainly correlated with the sulfur-containing precipitates (Fig. 3).

Another possible explanation for the higher corrosion rate of TP347HFG compared with S304HCu in oxyfuel gas may be the difference in the initial alloy microstructures. Owing to the slow bulk

diffusion, Cr transport along grain boundaries in the alloy plays an important role in the overall scale formation in austenitic steels.<sup>8</sup> This has the result that the oxidation behavior can be strongly affected by the steel grain size or by “imperfections” introduced by surface deformation.<sup>6</sup> Kim et al.<sup>6</sup> investigated the oxidation behavior of a model austenitic steel with addition of Cu and heat treated to achieve different average grain sizes. The authors found a clear difference in the oxidation rate in air with 20% water vapor at 700°C depending on the grain size of the samples; i.e., the oxidation rate decreased with decreasing average grain size. As seen in Fig. 7, the average grain size for S304HCu steel was smaller than for TP347HFG. This may be a more important factor governing the differences in oxidation rate of the two materials than the differences in minor alloying additions.

## CONCLUSION

During 1000 h of exposure of three selected austenitic steels at 650°C, the relative ranking of the corrosion resistance of the steels changed when the simulated test environment was altered from a standard, oxidizing flue gas to a reducing oxyfuel flue gas.

The 18 wt.% Cr austenitic steels S304HCu and TP347HFG formed a double-layer surface scale in the oxyfuel gas. Chromia scale was formed in the reducing gas with local formation of Fe-rich nodules. In the subscale region, Cr sulfide precipitates were formed, which tended to become oxidized, thus forming an internal mixed oxide/sulfide zone. This effect was found to be stronger for TP347HFG than for S304HCu. No indications of external sulfide or sulfate formation were found after 1000 h of exposure.

During exposure to the oxyfuel gas, external chromia scale formation was found for the 22 wt.% Cr austenitic steel Sanicro 25, and the corrosion rate was lower than for the 18% steels. Internal Cr sulfide formation and the resulting matrix Cr depletion did not cause substantial deterioration of the protective chromia base surface scale. In the reducing gas, however, local chromia formation was found along with regions forming external sulfides, mainly containing Ni and Cu. Apparently, the high concentration of Ni in Sanicro 25 allows formation of these rapidly growing sulfide phases, which adversely affect the formation of the protective Cr oxide, despite the higher Cr content of the steel. Beneath the external sulfide-containing scales, extensive internal oxidation of chromium was found to accompany internal sulfidation.

## ACKNOWLEDGEMENTS

The authors are grateful to Mr. Cosler for carrying out the oxidation experiments, Mr. Gutzeit and Mr. Bartsch for the metallographic investigations, and Dr. Wessel and Dr. Grüner for SEM analyses.



The authors also acknowledge financial support from the German Federal Ministry of Economics and Technology and the European Commission (Projects: “ADECOS-Komponenten” and “MAC-PLUS,” respectively).

## REFERENCES

1. T. Pikkarainen, A. Tourunen, and J. Hämäläinen, *Energy Mater.* 2, 78 (2007).
2. B.J.P. Buhre, L.K. Elliott, C.D. Sheng, R.P. Gupta, and T.F. Wall, *Prog. Energy Combust. Sci.* 31, 283 (2005).
3. K. Jordal, M. Anheden, J. Yan, and L. Strömberg, in *Proc. of 7th Int. Conf. on Greenhouse Gas Control Technologies (GHGT7)* (Vancouver, Canada, 5–9 Sept 2004), p. 201.
4. B. Bordenet and F. Kluger, *Mater. Sci. Forum* 595–598, 261 (2008).
5. W.J. Quadackers, P. Huczkowski, A. Gerhardt, U. Burchardt, A. Chyrkin, and T. Hüttel, in *Proceedings of 10th Liege Conference: Materials for Advanced Power Engineering* (Liege, Belgium, 2014), p. 820.
6. J.-H. Kim, B.K. Kim, D.-I. Kim, P.-P. Choi, D. Raabe, and K.-W. Yi, *Corros. Sci.* 96, 52 (2015).
7. W.J. Quadackers, T. Olszewski, J. Piron-Abellan, and L. Singheiser, *VDI-Ber.* 2102, 81 (2010).
8. W.J. Quadackers and J. Zurek, *Shreir's Corrosion* (Oxford: Elsevier, 2010), p. 407.
9. G.H. Meier, K. Jung, N. Mu, N.M. Yanar, F.S. Pettit, J. Pirón Abellán, T. Olszewski, L. Nieto Hierro, W.J. Quadackers, and G.R. Holcomb, *Oxid. Met.* 74, 319 (2010).
10. P. Huczkowski, D.J. Young, T. Olszewski, A. Chyrkin, and W.J. Quadackers, *Oxid. Met.* (2017). <https://doi.org/10.1007/s11085-017-9809-2>.
11. O. Bolland, H.M. Kvamsdal, and J.C. Boden, *Carbon Dioxide Capture for Storage in Deep Geologic Formations, Chapter 29*, vol. 1 (Amsterdam: Elsevier, 2008), p. 499.
12. P. Huczkowski, A. Chyrkin, L. Singheiser, W. Nowak, and W.J. Quadackers, in *NACE Corrosion 2016* (Vancouver, Canada, 2016), Paper No. 7391.
13. P. Huczkowski, S. Najima, A. Chyrkin, D. Grüner, and W.J. Quadackers, *Mater. High Temp.* 35, 275 (2018).
14. J. Zurek, E. Wessel, L. Niewolak, F. Schmitz, T.-U. Kern, L. Singheiser, and W.J. Quadackers, *Corros. Sci.* 46, 2301 (2004).
15. D.J. Young, *High Temperature Oxidation and Corrosion of Metals* (UK: Elsevier, 2008).
16. R.E. Lobnig and H.J. Grabke, *Corros. Sci.* 30, 1045 (1990).
17. C. Zhou, L.W. Hobbs, and G.J. Yurek, *High-Temperature Oxidation and Sulphidation Processes* (New York: Pergamon, 1990), p. 113.
18. S.-H. Choi and J. Stringer, *Mater. Sci. Eng.* 87, 237 (1987).
19. B. Gleeson, *Mater. Res.* 7, 61 (2004).
20. J. Zurek, S.-M. Yang, D.-Y. Lin, T. Huettel, L. Singheiser, and W.J. Quadackers, *Mater. Corros.* 66, 315 (2015).
21. T.D. Nguyen, J. Zhang, and D.J. Young, *Oxid. Met.* 81, 549 (2014).
22. P. Huczkowski, N. Christiansen, V. Shemet, L. Niewolak, J. Piron-Abellan, L. Singheiser, and W.J. Quadackers, *Fuel Cells* 6, 93 (2006).
23. D. Caplan, P.E. Beaubien, and M. Cohen, *Trans. Met. Soc.* 233, 766 (1965).